





## Quadriexcitons and excitonic condensate in a symmetric electron-hole bilayer with valley degeneracy

Stefania De Palo <sup>1,2,\*</sup>, F. Tramonto <sup>2,†</sup>, Saverio Moroni <sup>1,‡</sup> and Gaetano Senatore <sup>2,§</sup>

<sup>1</sup>CNR-IOM-DEMOCRITOS c/o SISSA (International School for Advanced Studies), via Bonomea 265, 34136 Trieste, Italy

<sup>2</sup>Dipartimento di Fisica, Università di Trieste, strada Costiera 11, 34151 Trieste, Italy



(Received 21 April 2022; accepted 19 January 2023; published 26 January 2023)

Using quantum Monte Carlo simulations we have mapped out the zero-temperature phase diagram of a symmetric electron-hole bilayer with twofold valley degeneracy, as a function of the interlayer distance  $d$  and in-layer density  $n$ . We find that the effect of the valley degeneracy is to shrink the region of stability of the excitonic condensate, in favor of quadriexcitons at small  $d$  and of the four-component plasma at large  $d$ , with minor effects on the value of the excitonic condensate fraction. The enclosure of the condensate in a density window possibly explains why anomalous tunneling conductivity, interpreted as a signature of condensation, is observed only between two finite values of carrier density in graphene bilayers. Our phase diagram may provide directions to select device parameters for future experiments.

DOI: [10.1103/PhysRevB.107.L041409](https://doi.org/10.1103/PhysRevB.107.L041409)

The idea that spatially separated electrons and holes provide an ideal playground for the observation of superfluidity/superconductivity was put forward long ago [1]. An equilibrium condensate, however, has long remained elusive in conventional electron-hole semiconductor bilayers [2–4], while it was observed in semiconductor electron-electron (hole-hole) bilayers [5–7] in strong perpendicular magnetic fields [8], i.e., in the quantum Hall regime. It was recently argued that excitonic condensation should be strongly enhanced in coupled electron-hole graphene bilayers, where extremely thin hexagonal boron nitride (hBN) barriers can be used [9] and electrons and holes have equal masses. Yet, carrier valley degeneracy is present in graphene bilayers and its effect is not immediately obvious; moreover, (i) a BCS mean field [10] would suggest an enhancement of the condensate, (ii) the screening by a larger number of fermion components would point to a weakening of the  $e$ - $h$  attraction, and (iii) the presence of four fermion components in each bilayer would allow for the formation of quadriexcitons [11].

Experiments on coupled graphene bilayers promptly followed the proposal in Ref. [9], replicating however the scenario encountered in semiconductor bilayers, with no evidence of a condensate in coupled electron-hole graphene bilayers [12,13] and clear evidence of a condensate in coupled electron-electron graphene bilayers in the quantum Hall regime [14,15]. Eventually, evidence of condensed interbilayer excitons in zero magnetic field, signaled by enhanced tunneling, was reported in coupled electron-hole graphene bilayers [16] and more recently in coupled monolayers of

transition metal dichalcogenides [17,18]; moreover, thermodynamic evidence of the condensate was also provided [19]. We should recall at this point that some evidence of condensation was also found in semiconductor electron bilayers, with long-lived indirect excitons produced by photoexcitation and electrostatic trapping [20,21] and in excitons coupled to light confined within a cavity (exciton polaritons), which do live long enough to condense and require a continuous input of light [22].

Here, we restrict ourselves to equilibrium excitonic condensation in systems of electron and holes and assess the effects of the interplay of the valley degeneracy  $g_v$ , the interlayer distance  $d$ , and the in-layer density  $n$  in determining the  $T = 0$  phase diagram of the system. To this end we resort to quantum Monte Carlo (QMC) simulations of the simplest possible model, i.e., a paramagnetic, symmetric electron-hole bilayer ( $m_e = m_h = m_b$ ,  $g_v = 2$ ), to mimic the situation encountered in double bilayer graphene [9]. In effective Hartree atomic units [ $\hbar = m_b = e^2/(4\pi\epsilon_0\epsilon) = 1$ ], which we use throughout, the Hamiltonian of the system reads

$$\begin{aligned}
 H = & -\frac{1}{2} \sum_{v,i} \nabla_{e,v,i}^2 + \frac{1}{2} \sum'_{v,v',i,i'} \frac{1}{|\mathbf{r}_{e,v,i} - \mathbf{r}_{e,v',i'}|} \\
 & -\frac{1}{2} \sum_{v,i} \nabla_{h,v,i}^2 + \frac{1}{2} \sum'_{v,v',i,i'} \frac{1}{|\mathbf{r}_{h,v,i} - \mathbf{r}_{h,v',i'}|} \\
 & - \sum_{v,v',i,i'} \frac{1}{\sqrt{|\mathbf{r}_{e,v,i} - \mathbf{r}_{h,v',i'}|^2 + d^2}}, \quad (1)
 \end{aligned}$$

where terms with both  $v' = v$  and  $i' = i$  are excluded from the primed sums and  $\mathbf{r}_{e,v,i}$  ( $\mathbf{r}_{h,v,i}$ ) is the in-plane position of the  $i$ th electron (hole) in valley  $v$ . Above,  $m_b$  is the band effective mass of the carriers, which move in a medium of dielectric constant  $\epsilon$ . QMC simulations of the  $g_v = 1$  case are already available both at  $T = 0$  [23–27] and at  $T > 0$  [28].

\*depalo@iom.cnr.it

†Present address: Kyndryl Italia Innovation Services S.r.l., Via Circonvallazione Idroscalo snc, 20090 Segrate (MI), Italy.

‡moroni@iom.cnr.it

§senatore@units.it

At a given valley degeneracy, the properties of the system depend on the interlayer distance  $d$  and the in-layer coupling parameter  $r_s = 1/\sqrt{\pi n}$ , while the ratio  $r_s/d$  measures the importance of the interlayer attraction, as compared to the in-layer repulsion. Provided that screening is not too strong, i.e.,  $r_s \gtrsim 1$ , a paired phase is expected for  $r_s/d > 1$  [23,25]. Moreover, for  $r_s/d \gg 1$  quadriexcitons [11] should appear, instead of the biexcitons found in the one-valley case [25]. In this Letter we systematically investigate the region  $r_s < 8$ , for systems with  $N = 84$  particles per layer. We also study some systems with a larger number of particles, up to  $N = 148$ , to assess size effects, as well as some systems at lower densities (larger  $r_s$  values).

We have employed variational and diffusion Monte Carlo [29–31] (VMC and DMC) as implemented in our own code. At each  $r_s$  and  $d$ , an optimal trial function  $\Psi_T$  is determined by minimizing the variational energy with respect to a number of optimizable parameters [32]. We then compute estimates of the properties of interest using Monte Carlo integration with  $|\Psi_T|^2$  as the *importance function* and, in most cases, using also the more accurate fixed-node DMC [29,30] with  $\Psi_T$  as the guiding function. We have used a singlet BCS-Jastrow trial function [23,33]

$$\Psi_T = J \prod_{\sigma} D_{e,h}^{\sigma,\sigma}, \quad (2)$$

$$D_{e,h}^{\sigma,\sigma} = \det[\phi(\mathbf{r}_{e,\sigma,i} - \mathbf{r}_{h,\sigma,j})], \quad (3)$$

with  $\sigma = (v, s_z)$  the valley-spin index or flavor, and the Jastrow factor

$$J = \exp \left[ -(1/2) \sum_{\mu,\mu'} \sum_{i_\mu, j_{\mu'}}' u_{\mu,\mu'}(|\mathbf{r}_{i_\mu} - \mathbf{r}_{j_{\mu'}}|) \right] \quad (4)$$

embodying two-body correlations. Above, the *species* index  $\mu = (t, \sigma)$  combines the particle type ( $t = e, h$ ) and the flavor; moreover, the primed sum for  $\mu' = \mu$  contains only the terms with  $i_\mu \neq j_\mu$ . The pairing orbital  $\phi(\mathbf{r})$  is chosen of a flexible form suggested earlier [25,34],

$$\phi(\mathbf{r}) = c(r) + \sum_{l=1}^{N_k} p_{|k_l|} \cos(\mathbf{k}_l \cdot \mathbf{r}), \quad (5)$$

where  $c(r)$  is a spherical function of finite range  $r_c \leq L/2$ ,  $L$  is the side of the periodic square simulation box, and the sum is over closed shells of the shortest reciprocal space wave vectors. The BCS part of the wave function  $\prod_{\sigma} D_{e,h}^{\sigma,\sigma}$  is able to describe different homogeneous fluid phases [25]. When  $p_{|k_l|} = 0$  for all  $l$ , one obtains a fluid of excitons. On the contrary, when  $c(r) = 0$ ,  $N_k = N/4$ , and  $p_{|k_l|} \neq 0$  for all  $l$ , one obtains a plasma phase described by plane-wave Slater determinants. In this latter case, in fact,  $D_{e,h}^{\sigma,\sigma} = D_e^{\sigma} D_h^{\sigma}$  [33] and  $D_i^{\sigma} = \det[\exp(i\mathbf{k}_l \cdot \mathbf{r}_{t,\sigma,i})]$ . The Jastrow factor, embodying two-body terms, apart from generally improving the wave function, is crucial in making possible polyexcitonic phases [35].

The function  $c(r)$  and all pseudopotentials  $u_{\mu,\mu'}(r)$  in the Jastrow factor are expanded on a flexible basis of locally piecewise-quintic Hermite interpolants [36], which among other things easily accommodates constraints at the end points. For each function its radial range and the expansion

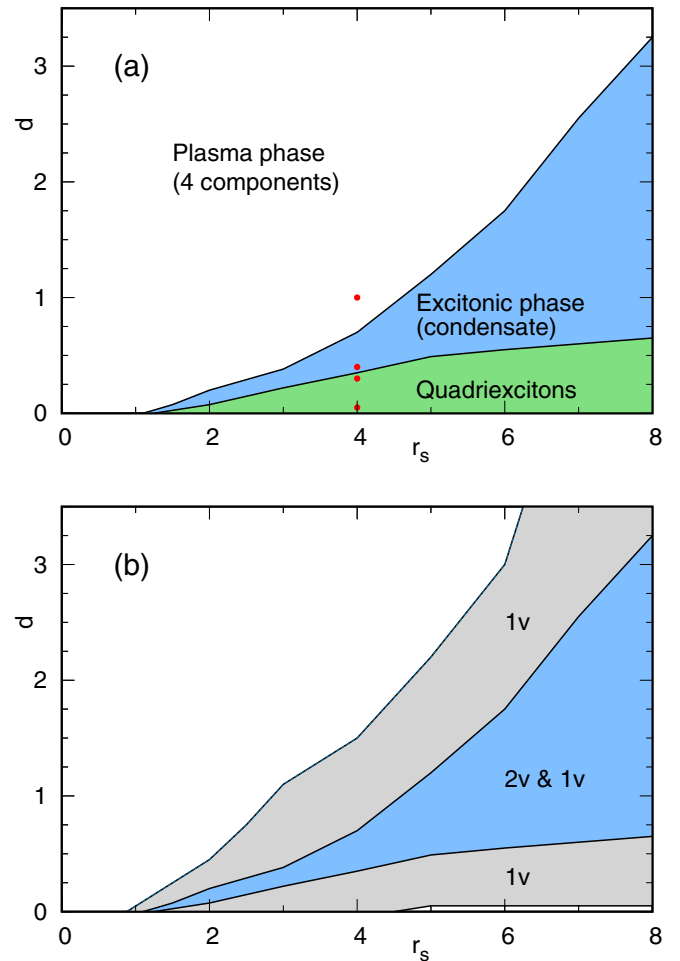


FIG. 1. (a) Phase diagram of an electron-hole bilayer with twofold valley degeneracy for small to moderate values of the intralayer coupling  $r_s$  and interlayer distance  $d$ . The red dots indicate states that are studied in Figs. 2 and 3. The regions of stability of the competing (fluid) phases are displayed in different colors. (b) Comparison of the phase diagrams of electron-hole bilayers with one (1v) and two (2v) valleys. The region of stability of the excitonic phase in the one-valley system [25,38] (union of the gray and blue areas) is substantially reduced in going to the two-valley system (blue area).

coefficients provide the variational parameters. For the pairing orbital  $\phi(r)$  such a set of variational parameters is augmented by the plane-wave coefficients  $p_{|k_l|}$ . Depending on the chosen numbers of knots in the radial mesh and plane-wave coefficients, the overall number of variational parameters used in the simulations described below is typically between about 50 and 60 [37].

The main outcomes of our DMC simulations are summarized in the phase diagram displayed in Fig. 1(a). For small values of the intralayer coupling  $r_s \lesssim 1$  (large density), a four-component plasma phase is found stable at all distances evidently due to strong screening. As one turns to larger values of  $r_s$  ( $r_s \gtrsim 1$ ) the interlayer attraction becomes more effective and stabilizes a novel quadriexcitonic phase at smaller distances and an excitonic phase with condensate

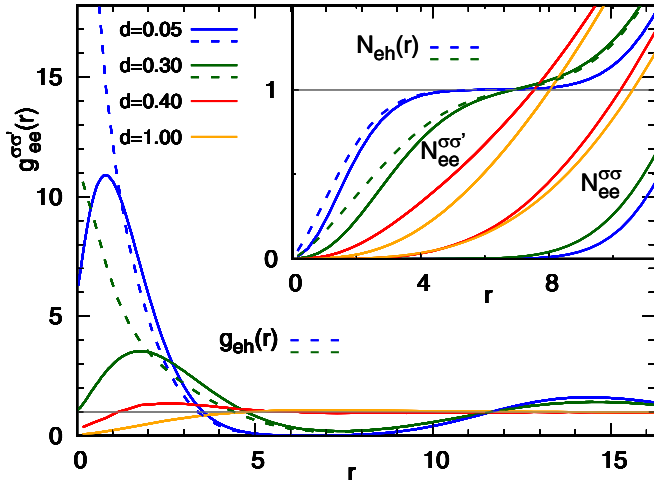


FIG. 2. PCFs (solid lines) between electrons (holes) with different flavors ( $\sigma' \neq \sigma$ ) in a symmetric electron-hole bilayer with twofold valley degeneracy, at  $r_s = 4$ ; interlayer distances  $d$  correspond to various phases (see Fig. 1). The inset reports the RCNs defined in Eq. (6). Electron-hole PCFs and RCNs are also shown for the two smaller distances (dashed lines), where they turn out to be independent of flavors, which have therefore been dropped.

at intermediate distances. As illustrated in Fig. 1(b), with respect to the findings of DMC simulations for a symmetric electron-hole bilayer without valley degeneracy [23,25] we obtain a substantial shrinking of the region of stability of the excitonic phase, especially at small  $r_s$ . This may partly explain the difficulties encountered in finding experimental evidence of excitonic condensation in coupled electron-hole graphene bilayers [12,13,16] and suggests avoiding high density in the search for the condensate, as has been noted before [9]; it also shows that the system without valley degeneracy appears to be a better choice for experiments aiming at the detection of an excitonic condensate. In the density range investigated here, we find no evidence of biexcitons [25], which appear to be substituted by the much more stable quadriexcitons [39]. Below we characterize the various phases by analyzing features of the extrapolated estimates of pair correlation functions and condensate fraction [37].

In Fig. 2 we report the pair correlation function (PCF) [37] between electrons with different flavors  $g_{ee}^{\sigma\sigma'}(r)$ ,  $\sigma' \neq \sigma$ , at  $r_s = 4$ . By symmetry,  $g_{ee}^{\sigma\sigma'}(r) = g_{hh}^{\sigma\sigma'}(r)$ . In the plasma phase ( $d = 1$ ) the PCF is structureless for  $r \gtrsim 5$ , with a modest correlation hole for  $r \lesssim 5$ . In the excitonic phase ( $d = 0.4$ ) the PCF remains structureless at larger distances, though showing a modest increase at smaller distances. As one crosses into the quadriexcitonic phase ( $d = 0.3$ ) a large peak (higher than 3) appears at small distances, followed by a deep wide minimum, inducing pronounced oscillations at large distances. This behavior is further enhanced at  $d = 0.05$  with a peak as large as 11 and a minimum of 0. So, what is causing an “effective attraction” between unlike flavor electrons (holes), that overcomes direct Coulomb repulsion and produces such a short-range ordering? We note that this phenomenon is accompanied by the fact that the electron-hole PCF  $g_{eh}^{\sigma\sigma'}(r)$ , which is strongly peaked on the electron, becomes independent on the flavor and displays the same deep wide minimum

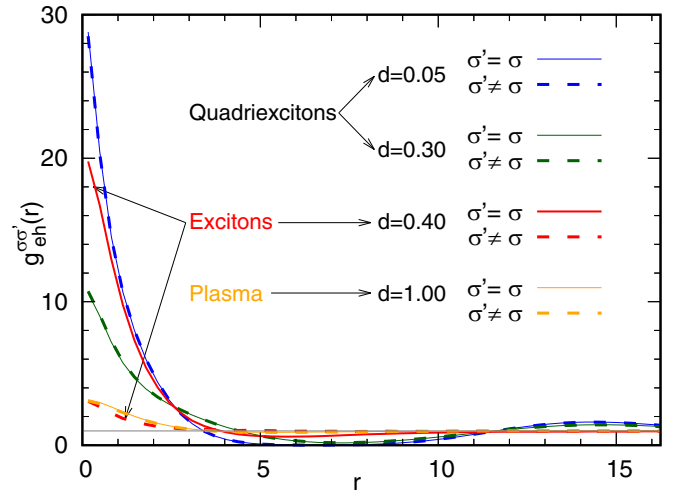


FIG. 3. Electron-hole PCFs in a symmetric electron-hole bilayer with twofold valley degeneracy, at  $r_s = 4$  and interlayer distances  $d$  corresponding to various phases (see Fig. 1). The PCFs of quadriexcitons and plasma are independent of flavors  $\sigma, \sigma'$ .

found in  $g_{ee}^{\sigma\sigma'}(r)$ ,  $\sigma' \neq \sigma$ . A clue to what is going on is provided by the inspection of the distance-dependent pileup of particles of the species ( $t', \sigma'$ ) around a particle of the species ( $t, \sigma$ ), i.e., the running coordination number (RCN),

$$N_{tt'}^{\sigma\sigma'}(r) = 2\pi n_{t',\sigma'} \int_0^r ds s g_{tt'}^{\sigma\sigma'}(s) \quad (6)$$

$n_{t,\sigma}$  being a species areal density.

In the inset of Fig. 2 we display  $N_{ee}^{\sigma\sigma'}(r)$  and  $N_{eh}^{\sigma\sigma'}(r)$ , respectively counting the average number of electrons (holes) with flavor  $\sigma'$  around an electron with flavor  $\sigma$ . Let us consider the case  $d = 0.05$  first. It is evident that electrons with the same flavor as the one at the origin are completely expelled from a very large region,  $N_{ee}^{\sigma\sigma}(r) \simeq 0$ ,  $r \lesssim 8$ . They make space for a dynamic compound of radius about 5, comprising 4 electrons (the one at the origin and 3 with  $\sigma' \neq \sigma$ ) and 4 holes of the four flavors. This is what we call quadriexciton. At  $d = 0.05$  the quadriexciton appears to be well defined, being neatly separated by its nearest neighbors, whereas at  $d = 0.30$  neighboring quadriexcitons touch and at  $d = 0.40$  they are melted into excitons.

The comparison in Fig. 3 of the electron-hole PCFs of the various phases at  $r_s = 4$  reveals in the excitonic phase a large difference between paired ( $\sigma' = \sigma$ ) and unpaired ( $\sigma' \neq \sigma$ )  $g_{eh}^{\sigma\sigma'}(r)$ , the height at the origin differing by as much as a factor 6. On the contrary,  $g_{eh}^{\sigma\sigma'}(r)$  is flavor independent both in the plasma phase, a consequence of the symmetry of the wave function, and in the quadriexcitonic phase, seemingly as an effect of the interplay of pseudopotentials and pairing orbital in the energy minimization. Such an interplay often results in a very repulsive pseudopotential  $u_{\mu,\mu}(r)$  between electrons (holes) with the same flavor, as found also in the biexcitonic phase of the one-valley system [25]. We remark that the qualitative features of PCFs and RCNs of the various phases illustrated above for  $r_s = 4$  are common to the whole density range displayed in Fig. 1.

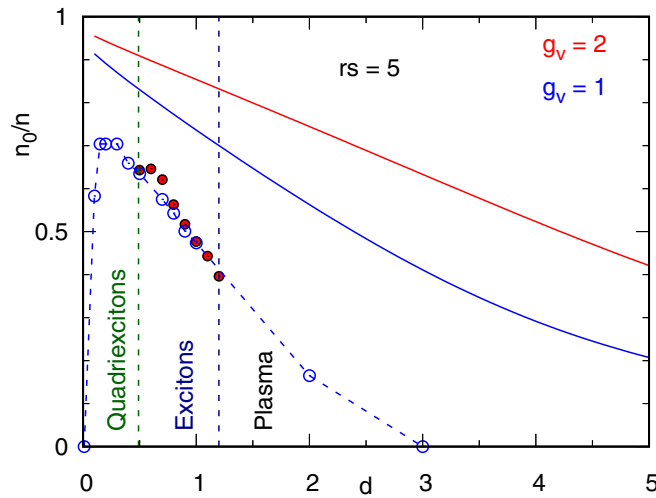


FIG. 4. Condensate fraction vs interlayer distance  $d$  in a symmetric electron-hole bilayer, at  $r_s = 5$ : (a) Present results for  $g_v = 2$  (red dots), with vertical dashed lines providing boundaries between phases; (b)  $g_v = 1$  [25] (blue circles), with the dashed blue line a guide to the eyes; (c) BCS mean field [10] predictions (solid curves).

The condensate fraction  $n_0/n$  in the excitonic phase is shown in Fig. 4 for  $r_s = 5$ , as a function of the interlayer distance  $d$  [37]. A comparison of the present results with those for the one-valley system [25] reveals that valley degeneracy, while substantially reducing the region of stability of the excitonic phase, leaves essentially unchanged the value of the condensate fraction. On the other hand, a comparison with the predictions of a BCS treatment [10] uncovers the limitations of such a mean-field approach, which predicts for the condensate a substantial increase with valley degeneracy and a much slower decay with the distance  $d$ . The results at  $r_s = 5$  are representative of our findings in the full range of density investigated in the present work, i.e.,  $r_s \leq 8$ , when one keeps in mind that (i) the stability window (in distance) of the excitonic phase grows with  $r_s$ , as it is clear from Fig. 1, and (ii) the condensate fraction becomes somewhat smaller than in the one-valley system at large densities ( $r_s < 3$ ).

The excitonic condensate at  $T = 0$  may be found in three regimes [40]: BCS at high density, BEC at low density, and BCS-BEC crossover in the middle. In order to characterize the regime for given  $d$  and  $r_s$  one may use the values of the condensate fraction  $n_0/n$  [27,41] and  $k_F r_{\text{ex}}$  [42], the ratio of the exciton radius  $r_{\text{ex}}$  and the interexciton distance  $\sim 1/k_F$ ,  $k_F$  being the Fermi wave vector of electrons. The exciton radius is evaluated as

$$r_{\text{ex}}^2 = 2\pi n_{h,\sigma} \int_0^{r_1} ds s g_{eh}^{\sigma\sigma}(s) s^2, \quad (7)$$

with  $r_1$  the radius of the circle centered on an electron containing on average one hole. In the density range studied here we find [37]  $0.21 \leq n_0/n \leq 0.75$  and  $0.31 \leq k_F r_{\text{ex}} \leq 0.96$  which, using the criteria of Refs. [27,41], places the condensate always in the BEC-BCS crossover regime.

We now turn to a peculiar aspect of the determination of the phase boundaries in Fig. 1(a). The wave functions obtained through energy minimization display a hysteresis

phenomenon when crossing a boundary. For the sake of clarity consider the quadriexciton to exciton transition at fixed  $r_s$ , which takes place at  $d_{qe}(r_s)$  and choose  $r_s = 4$ , where  $d_{qe}(4) = 0.35$ . If at  $d \gtrsim 0.35$  we start the energy minimization with a converged quadriexcitonic wave function taken from  $d < 0.35$ , the wave function remains quadriexcitonic in character, with zero condensate. However, by increasing  $d$  further the wave function eventually becomes excitonic, with a finite condensate. Similarly, if at  $d \lesssim 0.35$  we start with a converged excitonic wave function taken from  $d > 0.35$ , we find that the wave function remains excitonic; however, if we decrease  $d$  further, the wave function eventually becomes quadriexcitonic, with zero condensate. This implies that in the vicinity of  $d = 0.35$  we have two solutions with different character and different VMC energies as well as fixed-node DMC energies. The latter more accurate energies are thus used to determine the stable phase near the boundary [37].

To conclude, we comment on the correspondence of the calculated phase diagram [Fig. 1(a)] with interlayer conductance measurements in double-bilayer graphene-WSe<sub>2</sub> heterostructures [16]. In the experiment, a nominally divergent differential conductance between the two graphene bilayers, observed in a density interval  $(n_{\text{min}}, n_{\text{max}})$ , is attributed to the condensation of electron-hole pairs [16,17,43]. The suppression of condensation is ascribed to the in-plane screening of interlayer interactions for  $n > n_{\text{max}}$  and to disorder or competing phases for  $n < n_{\text{min}}$ , as generally expected for indirect excitons [44,45]. A disentanglement of disorder and quadriexcitons in suppressing the excitonic phase could in principle be achieved through measurements on samples with different degrees of disorder. We can relate the onset of pair condensation to phase transitions from plasma to excitons on the high-density side, which is common to one-valley electron-hole devices [17,25], and from quadriexcitons to excitons on the low-density side, which represents a mechanism peculiar to two-valley devices even in the absence of disorder [46]. We note that the large extent of the quadriexcitonic phase, compared to the biexcitonic phase in the one-valley system [25], is instrumental in having suppression of pair condensation at low density for interlayer spacings accessible experimentally.

The experimental observation of condensation is strongly peaked around conditions of balanced electron and hole densities [16], matching the symmetric two-valley system considered here. Other aspects of our model, such as the assumption of parabolic bands [47] and isotropic dielectric constant, are less faithfully representative of the actual heterostructure. Nevertheless, using the largest and the smallest dielectric constants [16] of the constituent materials to translate device parameters to our units, the experimental spacing between graphene bilayers varies from 0.1 to 0.5. This is well within the region where we find a nonzero condensate bracketed by the plasma and the quadriexciton phases.

Our results support and complement measurements of interlayer tunneling conductance [16,17,43] as a probe for indirect exciton condensation. Furthermore, they demonstrate the potential of graphene bilayer systems for the experimental investigation of thermodynamically stable, as opposed to optically pumped, multiexciton states.



- [1] Y. E. Lozovik and V. I. Yudson, Feasibility of superfluidity of paired spatially separated electrons and holes; a new superconductivity mechanism, *JETP Lett.* **22**, 274 (1975); A new mechanism for superconductivity: pairing between spatially separated electrons and holes, *Sov. Phys. JETP* **44**, 389 (1976).
- [2] U. Sivan, P. M. Solomon, and H. Shtrikman, Coupled Electron-Hole Transport, *Phys. Rev. Lett.* **68**, 1196 (1992).
- [3] A. F. Croxall, K. Das Gupta, C. A. Nicoll, M. Thangaraj, H. E. Beere, I. Farrer, D. A. Ritchie, and M. Pepper, Anomalous Coulomb Drag in Electron-Hole Bilayers, *Phys. Rev. Lett.* **101**, 246801 (2008).
- [4] J. A. Seamons, C. P. Morath, J. L. Reno, and M. P. Lilly, Coulomb Drag in the Exciton Regime in Electron-Hole Bilayers, *Phys. Rev. Lett.* **102**, 026804 (2009).
- [5] M. Kellogg, J. P. Eisenstein, L. N. Pfeiffer, and K. W. West, Vanishing Hall Resistance at High Magnetic Field in a Double-Layer Two-Dimensional Electron System, *Phys. Rev. Lett.* **93**, 036801 (2004).
- [6] E. Tutuc, M. Shayegan, and D. A. Huse, Counterflow Measurements in Strongly Correlated GaAs Hole Bilayers: Evidence for Electron-Hole Pairing, *Phys. Rev. Lett.* **93**, 036802 (2004).
- [7] J. P. Eisenstein and A. H. MacDonald, Bose–Einstein condensation of excitons in bilayer electron systems, *Nature (London)* **432**, 691 (2004).
- [8] Indeed, in an electron-electron bilayer at half filling in each layer, an electron-hole transformation in one of the two layers yields a compensated electron-hole bilayer [48].
- [9] A. Perali, D. Neilson, and A. R. Hamilton, High-Temperature Superfluidity in Double-Bilayer Graphene, *Phys. Rev. Lett.* **110**, 146803 (2013).
- [10] X. Zhu, P. B. Littlewood, M. S. Hybertsen, and T. M. Rice, Exciton Condensate in Semiconductor Quantum Well Structures, *Phys. Rev. Lett.* **74**, 1633 (1995).
- [11] J. S.-Y. Wang and C. Kittel, Excitonic molecules: A possible new form of chemical bonding, *Phys. Lett. A* **42**, 189 (1972).
- [12] J. I. A. Li, T. Taniguchi, K. Watanabe, J. Hone, A. Levchenko, and C. R. Dean, Negative Coulomb Drag in Double Bilayer Graphene, *Phys. Rev. Lett.* **117**, 046802 (2016).
- [13] K. Lee, J. Xue, D. C. Dillen, K. Watanabe, T. Taniguchi, and E. Tutuc, Giant Frictional Drag in Double Bilayer Graphene Heterostructures, *Phys. Rev. Lett.* **117**, 046803 (2016).
- [14] X. Liu, K. Watanabe, T. Taniguchi, B. I. Halperin, and P. Kim, Quantum Hall drag of exciton condensate in graphene, *Nat. Phys.* **13**, 746 (2017).
- [15] J. I. A. Li, T. Taniguchi, K. Watanabe, J. Hone, and C. R. Dean, Excitonic superfluid phase in double bilayer graphene, *Nat. Phys.* **13**, 751 (2017).
- [16] G. W. Burg, N. Prasad, K. Kim, T. Taniguchi, K. Watanabe, A. H. MacDonald, L. F. Register, and E. Tutuc, Strongly Enhanced Tunneling at Total Charge Neutrality in Double-Bilayer Graphene-WSe<sub>2</sub> Heterostructures, *Phys. Rev. Lett.* **120**, 177702 (2018).
- [17] Z. Wang, D. A. Rhodes, K. Watanabe, T. Taniguchi, J. C. Hone, J. Shan, and K. F. Mak, Evidence of high-temperature exciton condensation in two-dimensional atomic double layers, *Nature (London)* **574**, 76 (2019).
- [18] The suggestion to resort to coupled monolayers of transition metal dichalcogenides was put forward in Ref. [49].
- [19] L. Ma, P. X. Nguyen, Z. Wang, Y. Zeng, K. Watanabe, T. Taniguchi, A. H. MacDonald, K. F. Mak, and J. Shan, Strongly correlated excitonic insulator in atomic double layers, *Nature (London)* **598**, 585 (2021).
- [20] A. A. High, J. R. Leonard, M. Remeika, L. V. Butov, M. Hanson, and A. C. Gossard, Condensation of excitons in a trap, *Nano Lett.* **12**, 2605 (2012).
- [21] R. Anankine, M. Beian, S. Dang, M. Alloing, E. Cambril, K. Merghem, C. G. Carbonell, A. Lemaître, and F. Dubin, Quantized Vortices and Four-Component Superfluidity of Semiconductor Excitons, *Phys. Rev. Lett.* **118**, 127402 (2017).
- [22] J. Kasprzak, M. Richard, S. Kundermann, A. Baas, P. Jeambrun, J. M. J. Keeling, F. M. Marchetti, M. H. Szymańska, R. André, J. L. Staehli, V. Savona, P. B. Littlewood, B. Deveaud, and L. S. Dang, Bose–Einstein condensation of exciton polaritons, *Nature (London)* **443**, 409 (2006).
- [23] S. De Palo, F. Rapisarda, and G. Senatore, Excitonic Condensation in a Symmetric Electron-Hole Bilayer, *Phys. Rev. Lett.* **88**, 206401 (2002).
- [24] G. Senatore and S. D. Palo, Correlation effects in low dimensional electron systems: the electron-hole bilayer, *Contrib. Plasma Phys.* **43**, 363 (2003).
- [25] R. Maezono, P. López Ríos, T. Ogawa, and R. J. Needs, Excitons and Biexcitons in Symmetric Electron-Hole Bilayers, *Phys. Rev. Lett.* **110**, 216407 (2013).
- [26] R. O. Sharma, L. K. Saini, and B. P. Bahuguna, Ground state properties of electron-hole bilayer: Mass-asymmetric effect, *Phys. Rev. B* **94**, 205435 (2016).
- [27] P. López Ríos, A. Perali, R. J. Needs, and D. Neilson, Evidence From Quantum Monte Carlo Simulations of Large-Gap Superfluidity and BCS-BEC Crossover in Double Electron-Hole Layers, *Phys. Rev. Lett.* **120**, 177701 (2018).
- [28] J. Schleele, A. Filinov, M. Bonitz, and H. Fehske, Phase diagram of bilayer electron-hole plasmas, *Contrib. Plasma Phys.* **52**, 819 (2012).
- [29] P. J. Reynolds, D. M. Ceperley, B. J. Alder, and W. A. Lester, Fixed-node quantum Monte Carlo for molecules, *J. Chem. Phys.* **77**, 5593 (1982).
- [30] C. J. Umrigar, M. P. Nightingale, and K. J. Runge, A diffusion Monte Carlo algorithm with very small time-step errors, *J. Chem. Phys.* **99**, 2865 (1993).
- [31] W. M. C. Foulkes, L. Mitas, R. J. Needs, and G. Rajagopal, Quantum Monte Carlo simulations of solids, *Rev. Mod. Phys.* **73**, 33 (2001).
- [32] We have used the linear method [50,51] and checked, in selected cases, that the obtained minimum agrees with the one found by the improved stochastic reconfiguration method [52].
- [33] J. P. Bouchaud, A. Georges, and C. Lhuillier, Pair wave functions for strongly correlated fermions and their determinantal representation, *J. Phys. France* **49**, 553 (1988).
- [34] J. Carlson, S.-Y. Chang, V. R. Pandharipande, and K. E. Schmidt, Superfluid Fermi Gases with Large Scattering Length, *Phys. Rev. Lett.* **91**, 050401 (2003).
- [35] We have used four independent pseudopotentials  $u_{\mu,\mu'}$ , with appropriate cusp conditions [53]: same-flavor same-particle pairs, different-flavor same-particle pairs, same-flavor electron-hole pairs, and different-flavor electron-hole pairs.  $\phi(r)$  is taken cusplless.
- [36] V. Natoli and D. M. Ceperley, An optimized method for treating long-range potentials, *J. Comput. Phys.* **117**, 171 (1995).
- [37] See Supplemental Material at <http://link.aps.org/supplemental/10.1103/PhysRevB.107.L041409> for details of the simulations,

- optimization across phase boundaries, estimate of the condensate fraction, and structure of the quadriexcitons, which includes Refs. [23,25,54].
- [38] The boundary between plasma and excitonic phases in the one-valley system (upper green line), is estimated from the values of the condensate fraction available on an  $(r_s, d)$  grid [25].
- [39] We have preliminary results indicating that by increasing the distance from  $d = 0$  an isolated quadriexciton would dissociate into two biexcitons at  $d = 0.74$ . By increasing the distance farther, at  $d = 0.87$  a biexciton dissociates into two excitons [55,56]. In fact, with four flavors a dissociation of a quadriexciton into one triexciton and one exciton could also be possible.
- [40] A. J. Leggett, Diatomic molecules and Cooper pairs, in *Modern Trends in the Theory of Condensed Matter*, edited by A. Pekalski and J. A. Przystawa (Springer, Berlin, 1980), pp. 13–27.
- [41] A. Guidini and A. Perali, Band-edge BCS–BEC crossover in a two-band superconductor: physical properties and detection parameters, *Supercond. Sci. Technol.* **27**, 124002 (2014).
- [42] F. Pistolesi and G. C. Strinati, Evolution from BCS superconductivity to Bose condensation: Role of the parameter  $k_f \xi$ , *Phys. Rev. B* **49**, 6356 (1994).
- [43] I. B. Spielman, J. P. Eisenstein, L. N. Pfeiffer, and K. W. West, Resonantly Enhanced Tunneling in a Double Layer Quantum Hall Ferromagnet, *Phys. Rev. Lett.* **84**, 5808 (2000).
- [44] C. Comte and P. Nozières, Exciton Bose condensation: The ground state of an electron-hole gas - I. Mean field description of a simplified model, *J. Phys. France* **43**, 1069 (1982).
- [45] P. B. Littlewood and X. Zhu, Possibilities for exciton condensation in semiconductor quantum-well structures, *Phys. Scr.* **T68**, 56 (1996).
- [46] Quadriexciton condensation is also possible in principle, but we expect that enhanced mass, reduced density, and interaction-induced depletion will strongly suppress it relative to pair condensation.
- [47] S. Conti, A. Perali, F. M. Peeters, and D. Neilson, Multicomponent screening and superfluidity in gapped electron-hole double bilayer graphene with realistic bands, *Phys. Rev. B* **99**, 144517 (2019).
- [48] H. A. Fertig, Energy spectrum of a layered system in a strong magnetic field, *Phys. Rev. B* **40**, 1087 (1989).
- [49] M. M. Fogler, L. V. Butov, and K. S. Novoselov, High-temperature superfluidity with indirect excitons in van der Waals heterostructures, *Nat. Commun.* **5**, 4555 (2014).
- [50] J. Toulouse and C. J. Umrigar, Optimization of quantum Monte Carlo wave functions by energy minimization, *J. Chem. Phys.* **126**, 084102 (2007).
- [51] C. J. Umrigar, J. Toulouse, C. Filippi, S. Sorella, and R. G. Hennig, Alleviation of the Fermion-Sign Problem by Optimization of Many-Body Wave Functions, *Phys. Rev. Lett.* **98**, 110201 (2007).
- [52] S. Sorella, M. Casula, and D. Rocca, Weak binding between two aromatic rings: Feeling the van der Waals attraction by quantum Monte Carlo methods, *J. Chem. Phys.* **127**, 014105 (2007).
- [53] T. Kato, On the eigenfunctions of many-particle systems in quantum mechanics, *Commun. Pure Appl. Math.* **10**, 151 (1957).
- [54] N. D. Drummond, R. J. Needs, A. Sorouri, and W. M. C. Foulkes, Finite-size errors in continuum quantum Monte Carlo calculations, *Phys. Rev. B* **78**, 125106 (2008).
- [55] A. D. Meyertholen and M. M. Fogler, Biexcitons in two-dimensional systems with spatially separated electrons and holes, *Phys. Rev. B* **78**, 235307 (2008).
- [56] R. M. Lee, N. D. Drummond, and R. J. Needs, Exciton-exciton interaction and biexciton formation in bilayer systems, *Phys. Rev. B* **79**, 125308 (2009).